Journal of Materials Processing Technology 243 (2017) 170–183

Contents lists available at ScienceDirect

Journal of Materials Processing Technology

journal homepage: www.elsevier.com/locate/jmatprotec

Manufacturing of structured surfaces via grinding

E.J. Silva[a,*], B. Kirsch[b], A.C. Bottene[a], A. Simon[b], J.C. Aurich[b], J.F.G. Oliveira[a]

[a] University of Sao Paulo – USP, School of Engineering – Sao Carlos – EESC, Department of Production Engineering, Sao Carlos, SP, Brazil
[b] University of Kaiserslautern, Institute for Manufacturing Technology and Production Systems, P.O. Box 3049, 67653, Kaiserslautern, Germany

ARTICLE INFO

Article history:
Received 8 April 2016
Received in revised form 9 December 2016
Accepted 11 December 2016
Available online 13 December 2016

Keywords:
Grinding
Structuring
Surface
Dressing
Tool development
Tribology

ABSTRACT

This paper presents the possibilities and limitations of structuring surfaces using special grinding wheels. Two methods were evaluated. Workpieces were structured using a patterned grinding wheel, specially conditioned during the dressing operation. The second method uses a grinding wheel with defined grain pattern to produce structured surfaces with micro features. The obtained results indicated the feasibility of the two methods.

1. Introduction

In the scenario of modern manufacturing, with the current demand for products and processes that require minimum consumption of resources and in a sustainable way, the performance of a machined component regarding energy performance is of high interest. In bearings, for instance, surface characteristics can highly influence the energy loss or load capacity. Surface characteristics can also play important roles in terms of energy or signal transmission by defining the mechanisms and the kinematics involved in this exchange phenomena in a micro and nano scale (Bruzzone et al., 2008). For example, tribological properties are highly influenced by the degree of interaction between two surfaces, leading to different results of friction, wear and/or lubrication conditions with a direct impact on energy consumption. As presented by Ibatan et al., surface texturing for increasing the tribological performance of sliding components is a very active research field, with several contributions over the last decades, in terms of production methods, analysis of the tribological enhancements and prediction of the obtained results by simulation (Ibatan et al., 2015). The importance of structured surfaces can be seen in other areas, with recent application examples in electronics (Wang et al., 2015), optics (Cho et al., 2013) and health (Zhang et al., 2015).

Structured surfaces are commonly produced by applying optical or X-ray lithography, etching and laser ablation. Hilgenberg and Steinhoff (2015) presented a new approach to produce deterministic structures in skin-pass rolls used in the final forming operation of metal sheets for automotive applications using pulsed laser dispersing. Costa and Hutchings (2009b) developed a maskless electrochemical method to produce textured surfaces in metallic workpieces, in which 100 holes of 220 μm in diameter, arranged in a 10 × 10 mm configuration were etched, achieving a maximum depth of 45 μm, with cycle time of 60 s. Zhang and Meng (2012) studied the surface texturing of mild carbon steel (ASTM 1020) using photochemical machining, which consisted of eight main steps, from cleaning to photoresist removal. Circles and triangles were produced at micrometric scale, with dimensions ranging from 20 to 200 μm and hypotenuse length from 18 to 600 μm, respectively, with maximum depth of around 55 μm, after 900 s etching time.

When compared to the previous approaches, grinding is a promising alternative for surface structuring, as no additional investments in machine tools or manufacturing steeps are needed. The present manufacturing chains of sliding components where structured surfaces can be used to improve tribological properties mostly already include grinding. In order to produce a structured ground surface, the desired pattern has to be generated in the wheel surface itself and subsequently transferred to the workpiece during grinding. Different methods have been researched to produced a structured grinding wheel, but leading to limitations on the achieved structured surfaces. In 1989, Stepién presented a method for the production of structures by grinding in which a conventional grinding wheel was dressed with deep single or double helical grooves in a combination of dressing passes (Stępień, 1989). The

* Corresponding author.
E-mail address: eraldojs@sc.usp.br (E.J. Silva).

http://dx.doi.org/10.1016/j.jmatprotec.2016.12.009
0924-0136/

regular surface textures were limited to three basic shapes, requiring one or two grinding cycles with preselected grinding conditions, being a combination of the nominal active surface of the wheel and the stochastic arrangements of the abrasive grains (Stępień, 2011). Denkena et al. applied grinding to generate riblet structures in turbine blades to enhance performance (Denkena et al., 2010). Wheel microprofile geometry was dressed using a diamond profile roller, requiring two consecutive plunge dressing cycles with axial shift to achieve the desired riblet structure, increasing dressing time. Uhlmann et al. used a kinematic modulation of the grinding process to produce microstructures in ball bearings (Uhlmann et al., 2013).

Aiming at achieving an increased flexibility in terms of production of structured surfaces via grinding in combination with functional surface parameters, two different texturing methods are presented here. The first includes specially dressed grinding wheels, structured using a combination of a high-speed dressing axis and a texturing software for production of macro features. The second uses grinding wheels with pre-defined grain pattern to produce micro features in which several texturing types can be obtained by reproducing target-grinding conditions previously calculated via simulation for flat surfaces.

The approaches were developed in a research project in the scope of the Brazilian-German Collaborative Research Initiative on Manufacturing (BRAGECRIM). By covering micro (German project) and macro (Brazilian project) features in this binational research project, the findings on manufacturing structured surfaces via grinding can be transferred to all workpiece geometries relevant for sliding components.

2. Production of macro features using a random grain distribution wheel, specially conditioned during the dressing operation

2.1. Method

The developed method consists of two basic steps: patterning an of-the-shelf grinding wheel during dressing and transferring the pattern to the workpiece during grinding. Full details on the developed method can be found in Oliveira et al. (2010) and Silva et al. (2013). For patterning the wheel, the dressing depth (a_d) is dynamically changed according to the desired feature to be produced (Fig. 1). A high-speed axis, perpendicular to the wheel surface, was added to the dressing tool and was used to perform the modified dressing operation. The patterning software is used to generate the control signals for the high-speed axis based on the texture to be produced. Dressing time is not affected by the developed technique when compared to a regular dressing operation, as dressing and patterning can be done simultaneously in the same dressing stroke. Once the wheel is patterned, the desired feature has to be transferred to the workpiece during grinding. An integer speed ratio between wheel (n_s) and workpiece (n_w) has to be selected in order to insure proper pattern transferring. If not, the pattern will be erased in the subsequent workpiece rotation. The number of patterns in the workpiece can be scaled up according to the selected value of the speed ratio. One important point in this process to be described is that there is no need for a synchronization control system to keep the phase angle between grinding wheel and workpiece during processing (Oliveira et al., 2010). This synchronization is automatically obtained, but would need relevant patterned area to be stable. It works like a gear engagement effect.

In order to verify the consistency of the pattern imprint in the wheel surface, the acoustic emission (AE) mapping of the wheel surface Oliveira and Dornfeld (2001) is used. Fig. 2a shows the output result of a dressing pattern operation, in terms of AE [V_{rms}] values,

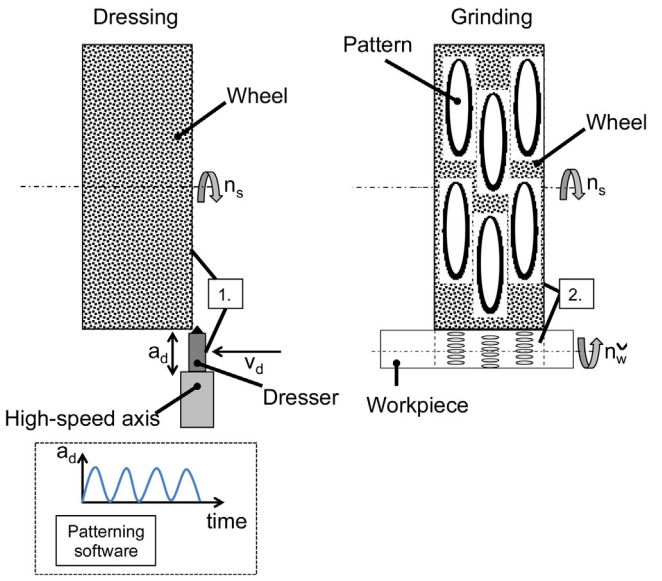

Fig. 1. Basic steps for manufacturing of structured surfaces via grinding using wheels conditioned during dressing: 1) patterning the wheel; 2) pattern transfer during grinding.

converted into a color intensity scale. The AE [V_{rms}] means the Root Mean Square value (in Volts) of the amplified signal. This value is correlated to the acoustic energy of the interaction between the dressing tool and the abrasive grains. The time constant used in the RMS calculation was of 0.2 microseconds. The vertical dimension represents the circumferential length of the grinding wheel and the horizontal one the wheel width. A pattern type "pockets" was inscribed into the wheel surface. The darker areas represent the lack of contact between the wheel and the dressing tool (pocket valleys). The brighter areas indicate the higher contact intensity regions (pocket peaks). For comparison, Fig. 2b presents an acoustic map of a non-patterned grinding wheel, indicating the homogeneity of contact interaction between dressing tool and grinding wheel.

The resulting macro features in the workpiece are strongly influenced by the process kinematics. Fig. 3 presents pattern transfer during grinding from the wheel to the workpiece, with emphasis on the resulting macro features dimensions:

As previously mentioned, to insure proper pattern transferring, an integer speed ratio between wheel and workpiece has to be selected. The feature width on the part (b_w) is not affected by the selected speed ratio, being equal to the feature width on the wheel (b_s). On the other hand, the feature length on the part (L_w) is depend on the adopted wheel and part velocities, according to Eq. (1)

$$L_w = \frac{L_s * v_w}{v_s} \quad (1)$$

where: L_s is the feature length on the wheel, v_s is the wheel speed and v_w is the workpiece speed

The next important feature dimensions to be defined are the resulting feature profile in the part and the feature depth (h_k). Fig. 4 presents an extraction of a linear plot of a roundness trace for a cylindrical part, indicating the major features of a pocket-type profile.

The profile shape and depth depend on the process kinematics and the dimensions involved. Fig. 5 presents the schematic representation of the cutting path for an idealized structured grinding wheel (Silva et al., 2016).

For this kinematics representation, the wheel is modeled as a milling cutter with the abrasive grains representing the cutter teeth equally spaced at a distance L. The depth of cut is the dimension a and the feature depth is denoted as h_k. The wheel is dressed with

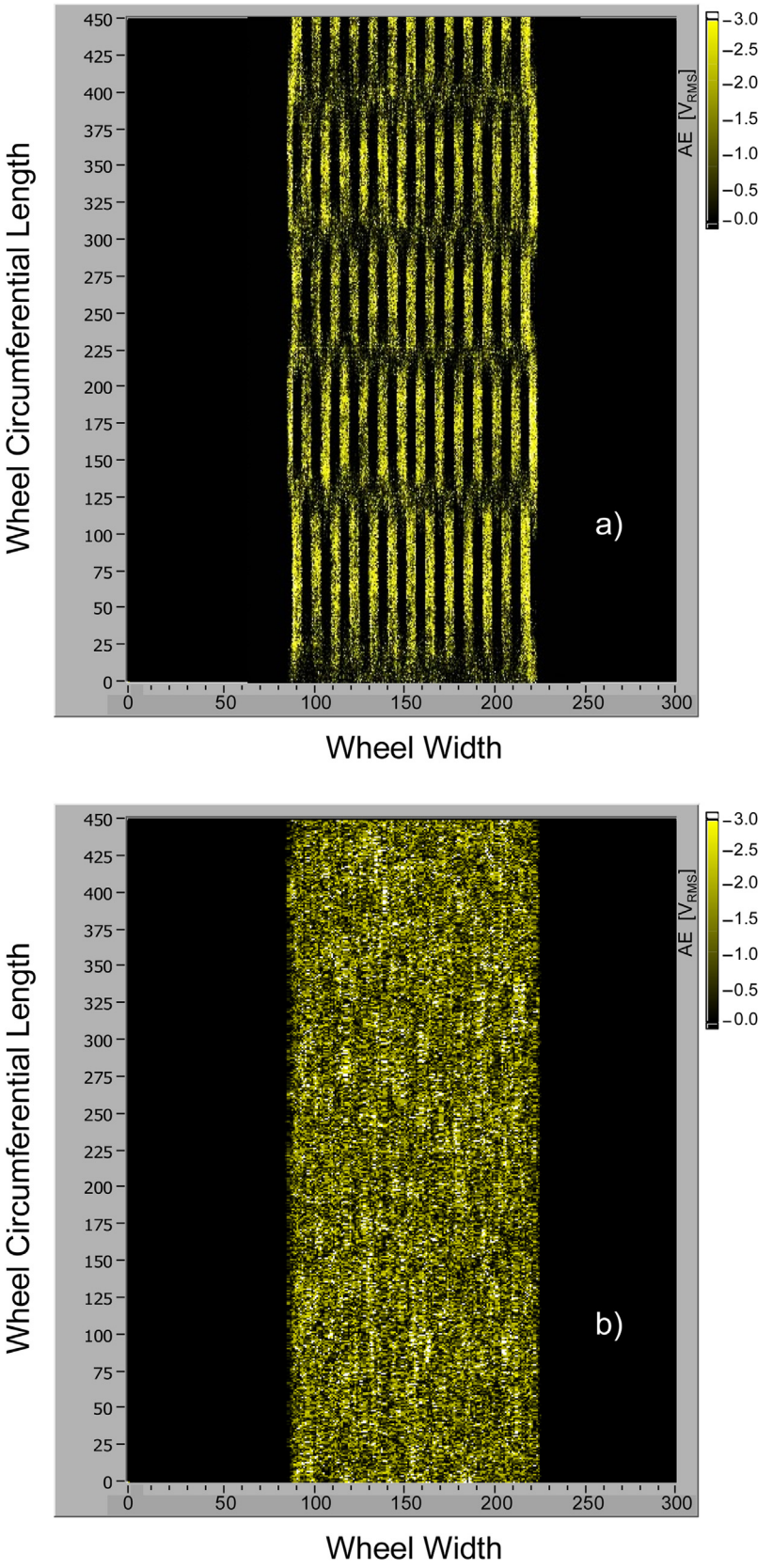

Fig. 2. Acoustic emission maps. a) patterned grinding wheel type “pockets”; b) non-patterned grinding wheel.

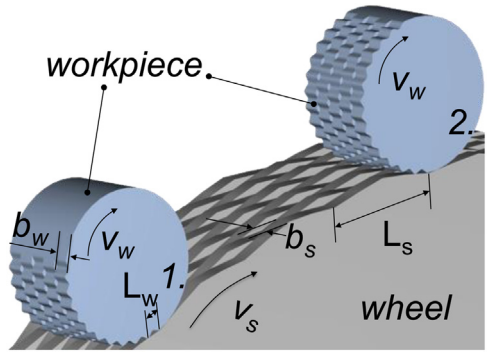

Fig. 3. Workpiece patterning and influence of grinding kinematics (Adapted from Oliveira et al., 2010).

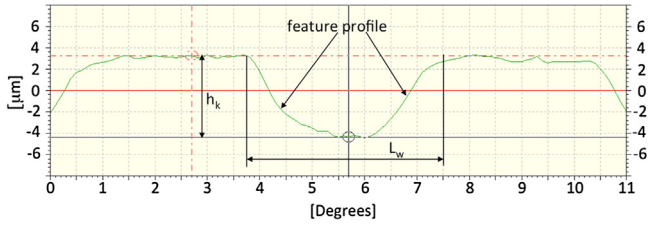

Fig. 4. Linear plot of a roundness trace of a pocket-type pattern profile.

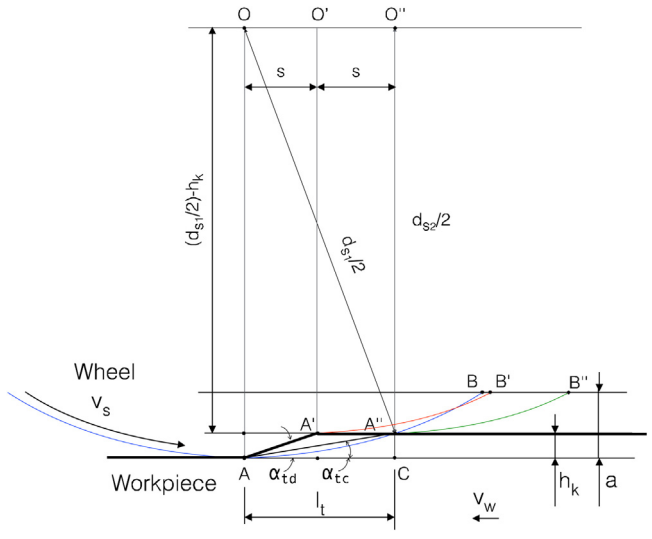

Fig. 5. Schematic representation of the cutting path for an idealized structured wheel (Silva et al., 2016).

a linear reduction in radius from diameter ds_1 to ds_2, leading to an increase in the workpiece size along the segment A-A'. Thus, the dimension h_k will be given by Eq. (3):

$$\boldsymbol{h_k} = \frac{\boldsymbol{d_{s1}} - \boldsymbol{d_{s2}}}{2} \tag{3}$$

By considering the last outermost cutting point of the grinding wheel in an up-grinding configuration, the cutting path starts at *A*, ending at point *B*, centered in *O*, with a depth of cut equal to *a* (blue curve). The first innermost cutting point of the wheel, displaced at a distance *s* from *O*, describes a curve path from *A*' to *B*', centered in *O*' with a depth of cut that can vary from zero to a-h_k (red curve). The desired profile angle will not be produced, as the grain will not touch the final surface of the part.

Two important angles can be identified in Fig. 5: the critical cavity step angle (α_{tc}) and the design cavity step angle (α_{td}), the last

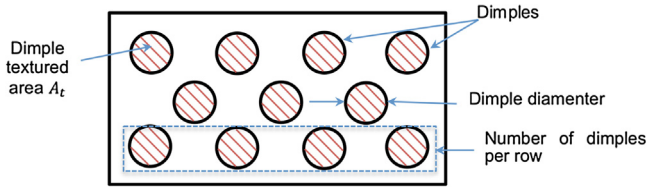

Fig. 6. Sketches of diples arrangement.

being a design parameter set during the patterning dressing. The critical cavity step angle (α_{tc}) will be defined by the curve path described by the first innermost abrasive grain being able to cut from *A*". The green curve path represents a consecutive grain being able to cut the depth of cut equal to a-h_k. Due to the magnitude of the dimensions involved, the segment *A*-*A*" can be approximated as a straight line. Thus, α_{tc} can be calculated by Eq. (4):

$$\alpha_{\boldsymbol{tc}} = \tan^{-1}\left(\frac{\boldsymbol{h_k}}{\boldsymbol{l_t}}\right) \tag{4}$$

Where, the value of l_t, can be given by Eq. (5)

$$\boldsymbol{l_t} = (\boldsymbol{h_k d_{s1}})^{1/2} \tag{5}$$

Both parameters α_t and l_t are primary ones for cavity design. Eq. (5) can be applied to cylindrical grinding by considering the equivalent diameter (d_e) instead of d_{s1}.

Due to contact kinematic limitations, not always the design cavity step angle α_{td} can be achieved, as α_{td} maximum value is limited by α_{tc}. In that case, the wheel contact kinematics will produce a rounder profile with a lower angle and increased pocket width. High equivalent wheel diameter limits maximum achievable angles.

2.2. Tested patterns

Dimples and chevrons are common features of the textured surfaces researched in the scientific community. Costa and Hutchings (2009a) evaluated the effects of surface texturing using dimples and grooves in a strip-drawing test. Galda et al. (2009) performed friction tests with block-on-ring friction machine using test specimens textured with pockets cavities of diameter equal to 900 µm and depth of 60 µm for improved oil retention.

For the present research, two different types of patterns were investigated: Dimples were imprint in a chessboard arrangement, as depicted in Fig. 6. The variation parameters in the dimples pattern type were the dimple diameter, number of dimples per row and the number of rows, resulting in different percentile of textured area (*S*) in respect to the total surface area of the workpiece.

In Fig. 7, the geometrical parameters for defining each chevron are presented, where: *a* is the chevron width, *b* is the total feature height (including the clearance between rows, *d*), *c* is the chevron thickness, *x* is the complementary chevron height and α is the chevron angle. Chevrons were designed to be oriented as a fish-bone structure, in which the chevron thickness, angle, number of chevrons per row and number of rows were controlled, aiming the variation of the percentile of textured area (*S*) in respect to the total workpiece surface area.

Once the primary design of the patterns was defined, the controlling dimensions of the features were selected. Wang et al. (2003) tested round micro-pits arranged in a square array with depths ranging from 2.4 to 16.6 µm, in SiC specimens. Deeper structures can lead to turbulences inside the structure. This will result in no additional pressure buildup, for example to increase the load capacity. There is also a risk of reduction or collapse of the lubricant layer (Mourier et al., 2006). Thus, for the dimples and chevrons tested in this research work, the features depth was selected based on pos-

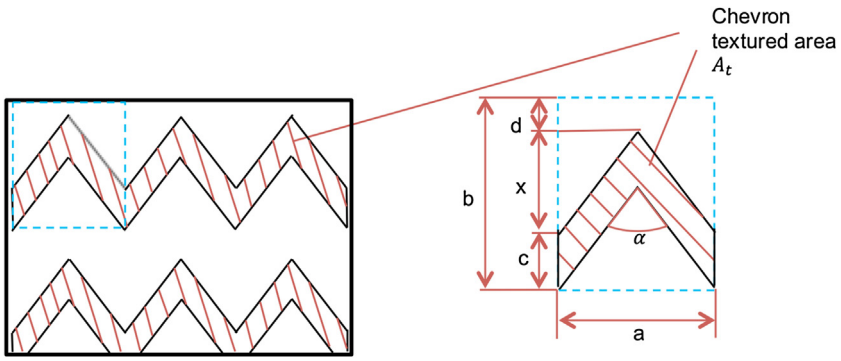

Fig. 7. Sketch fishbone structure.

sible industrial application, in which patterns will be produced in shafts that will be coupled into hydrodynamic bearings. Considering a clearance of 50 μm in radius when assembled, pattern depths were set to 1/10 of the clearance, leading to a target depth of 5 μm. Also, the wheel dressing system for patterning gives more stable performance at this range.

Another parameter is the ratio between the textured surface area compared to the non-textured one. Galda et al. (2009) found that the best percentage of textured surface area using dimples is between 10 and 15%. Tests were performed up to 20% in the aforementioned study. At this value, the results were not preferable. This does not include the chevrons. In terms of chevrons, it is assumed that the percentage of textured area, resulting in good properties obtained by the texture, is between 40 and 50% (Costa and Hutchings, 2007). Tables 1 and 2 present the range of the geometrical parameters for the dimples and chevrons that were produced, respectively.

2.3. Tools and materials

A cylindrical plunge grinding operation was performed for producing patterned workpieces. Prior to grinding, a vitrified bond aluminum oxide grinding wheel (55A46-1-K8VC1) was dressed using a MCD single-point dresser to produce the desired patterns in the wheel surface, with the following dressing conditions: dressing overlap (U_d) = 12; radial dressing depth (a_d) = varies (maximum 30 μm, as defined by the software); dressing lead (S_d) = 0.1 mm/rot, cutting speed (v_s) = 30 m/s. Dressing of conventional wheels is performed at a depth of cut of 20–40 μm. Normally, for a worn grinding wheel, the depth of cut is not really constant, since the wear produced by grinding leads to actual depth of cut variations. In the case presented in the paper, the depth variation is of about 5 in 30 μm. It is known that deeper dressing results in a sharper wheel surface with lower edge density up to a limited value. Previous tests showed that, for the same dressing lead, dressing depths above 20 μm don't produce significant changes in the wheel sharpness or edge density. In this case, the surface generated by the diamond inside the dimples (outer surface of the wheel dressed with the minimum value of dressing depth), may be a little smoother than the rest of it.

The ground workpiece material was AISI 4140, annealed. A particular shaft design was developed, in which interchangeable bushings could be coupled, patterned and further demounted for pattern inspection. Fig. 8 presents the shaft and bushing design and the test arrangement in the grinding machine.

The feasibility and limits of producing the dimples and chevrons using the proposed technique was evaluated by inspecting the obtained surface and comparing it to the design requirements. Besides, the proper measurement and separation of surface roughness parameters and texture depth is mandatory for the produced surfaces with hydrodynamic properties. The core roughness, peak (run-in zone) and the deep valleys regions (lubricant zone) have to be analyzed separately. For that, the set of R_k parameters (DIN 4776 and ISO 13565-2) were determined by measuring the obtained surface profile using a profilometer (TalySurf 50–Taylor Hobson) and being graphically extracted from the Bearing Area Curve (BAC). Additional parameters were added to the analysis (Silva et al., 2013): The core roughness parameter (R_k) was decoupled into two: top and bottom core roughness of the pattern geometry, R_{k0} and R_{k1}, respectively. The pattern depth (H_k) was also introduced, being the distance between half of the depth of the core roughness ranges ($R_{k0}/2$) and ($R_{k1}/2$).

R_{pk} and R_{vk} parameters were also derived from the Bearing Area Curve (BAC) computed within the evaluation length of the profile. To calculate the R_{pk}, a straight line having the smallest slope was fitted to a range of 40% along the abscissa corresponding to 40% of the points in the roughness profile of the top core roughness (R_{k0}). The line was then extended to 0% and 100% and two horizontal intersection lines were drawn where the fitted line intersects 0% and 100%. The 0% line separates the protruding peaks from the top core roughness profile. The area between the 0% line and the BAC is the peak area A_1. The point in which the 0% line intercepts the BAC defines the material ratio M_{r1}, separating the protruding peaks from the top core roughness profile. R_{pk} is then calculated as the height of the right angle triangle, which has the same area as the peak area A_1 and has M_{r1} as its base. The same approach was used to determine R_{vk}, now considering the bottom core roughness (R_{k1}) and by calculating the valley area A_2 and the material ratio M_{r2}. R_{pk} (the so called 'running surface roughness'), will quickly be worn away when two surfaces are sliding against each other. Thus, this value has to be minimized when designing tribological surfaces. On the other hand, high values of R_{vk} are desired, to increase oil-retaining capability, being recognized as a lubricant capacity indicator.

In addition to the BAC curve analysis, the obtained patterned surface was analyzed using a 3D measuring laser confocal microscope (LEXT, Olympus OLS4100). The part roundness was also measured (Talyrond 131–Taylor Hobson) and the uniformity of the pattern distribution around its circumference was evaluated.

2.4. Results and discussion

Fig. 9 presents the characterization results in terms of images of the obtained surface and the roundness plots when producing round dimples and varying the percentage of textured area (S).

Successful pattern formation was obtained for the first three tested conditions, in which the target number of patterns can be identified in the roundness plot. There was a decrease in the dimple depth with the increase of the percentage of textured area (S). This happened due to higher frequency required for the increase in the percentage of textured area and the limited frequency response

Table 1
Geometrical parameters for round dimples.

Depth [μm]	Radius [mm]	Number of dimples per row	Number of rows	percentile of textured area (*S*) [%]
5	1	11–68	11 and 23	10.05–62.13

Table 2
Geometrical parameters for chevrons.

Depth [μm]	a [mm]	b [mm]	c [mm]	d [mm]	Chevron angle α [°]	Number of chevrons per row	Number of rows	percentile of textured area (*S*) [%]
5	2.875, 23	2.875, 23	0.587–10.35	0.575	80–140	54	8	19.26–58.34

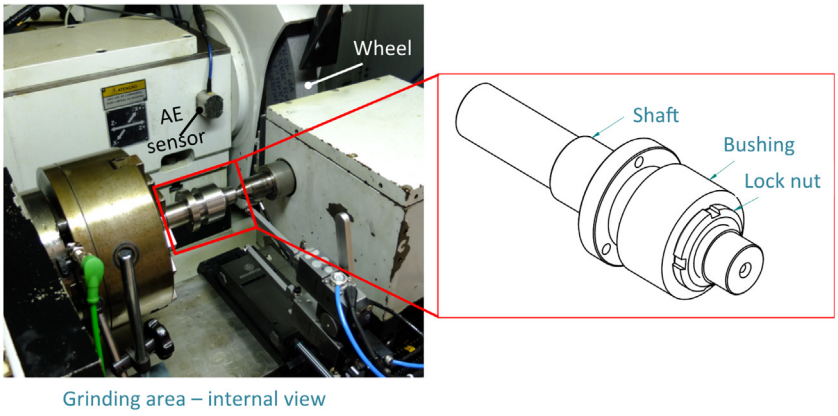

Fig. 8. Grinding test setup for patterning round workpieces.

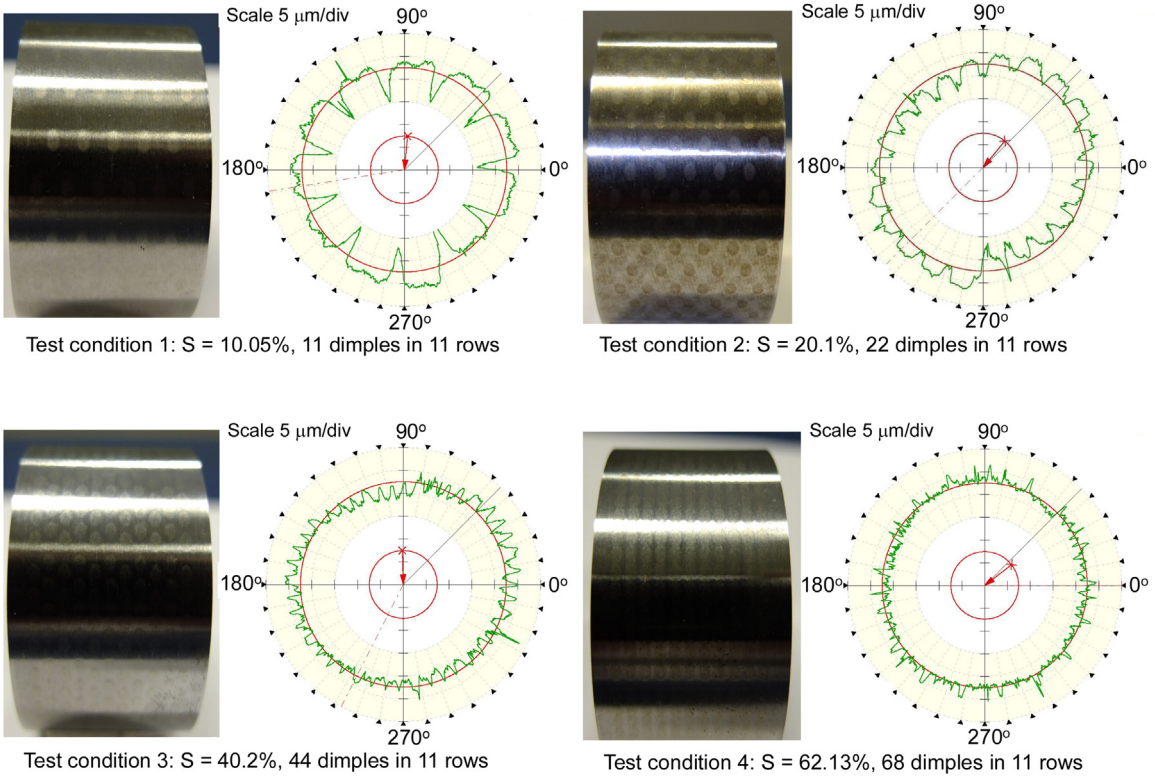

Fig. 9. Surface images and roundness plots of round dimples with different values of the percentage of textured area (*S*).

of the dressing displacement actuator. The process limitation for the given geometrical condition tested (grinding wheel diameter, d_s, 500 mm and workpiece diameter, d_w, 50.15 mm) was achieved in the condition S = 62.13%, that represented the manufacturing of 68 dimples per row. Process conditions were insufficient to keep self-synchronization and pattern overlap occurred.

The self-synchronization between wheel and part during the grinding process is a mandatory condition to achieve successful

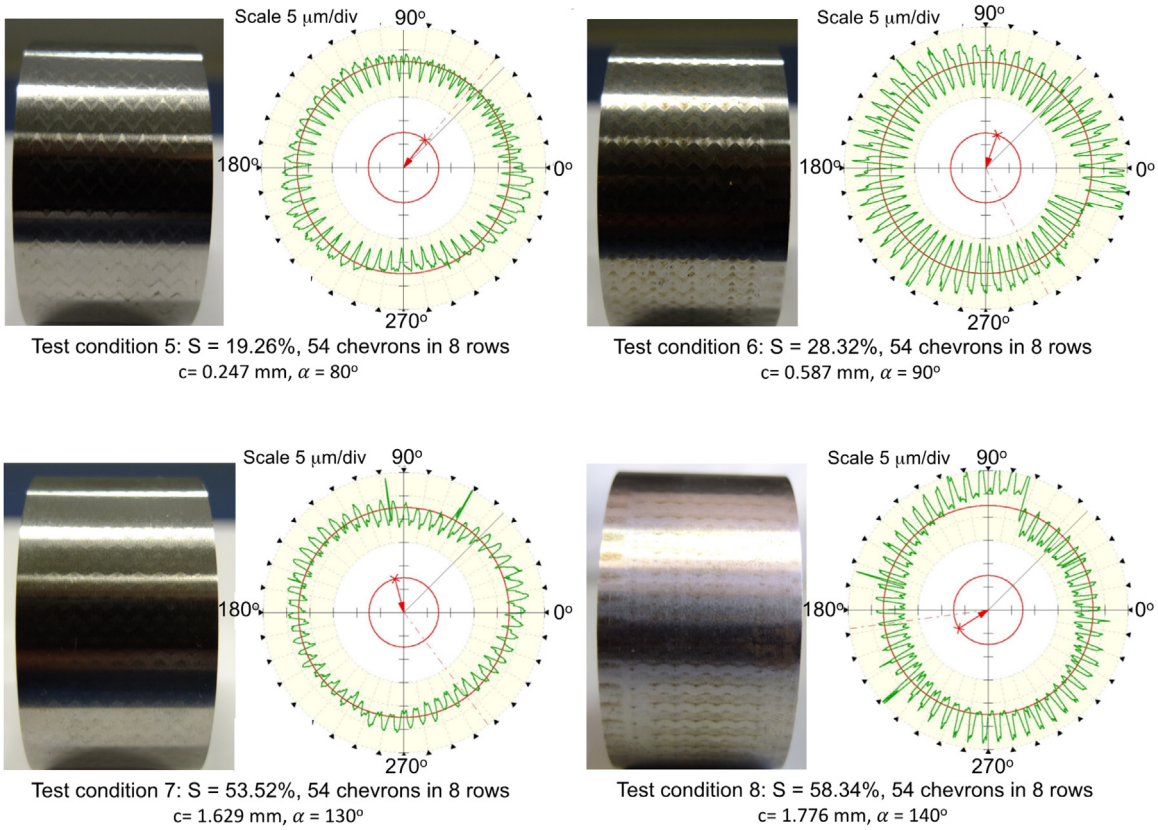

Fig. 10. Surface images and roundness plots of chevrons (fishbone arrangement) with different values of the percentage of textured area (S).

pattern transfer. This phenomenon can be illustrated as follows. Due to the small variations in the wheel or workpiece nominal rotations at each workpiece revolution, a shift in the engagement position between wheel and workpiece occurs and the wheel starts cutting a little earlier regarding the workpiece position. In the scenario of engagement position shift (change in the phase angle between wheel and part), the pattern will be ground a little in advance in every part rotation. If the phase angle shift is below a certain limit or the size and depth of the feature are big enough to ensure interlock between wheel and part in the level of the contact arc, there's a tendency of the wheel-workpiece system to find a stable position and no profile overlapping occurs, meaning that a self-synchronization is achieved. That mandatory condition was fulfilled in test conditions 1–3. Further investigation and additional tests would be needed to identify the causes of lack of self-synchronization in test condition 4.

Therefore, the self-synchronization depends on the capacity of the engagement between wheel and workpiece to produce tangential forces that keep the phase angle between those two elements. As the percentage of texture area increases, the dimple depth decreases leading to a weaker engagement.

Similar analysis was performed to the chevron patterns (Fig. 10). The fishbone structure was successfully formed in all tested conditions. The increasing in the percentage of the textured area was achieved by keeping constant the number of chevrons per row (54) and the number of rows (11) but changing the chevron angle (α) and thickness (c). Process limitation was detected for S = 58.34%, in which more severe burnout was detected due to the very fine dressing condition adopted (U_d = 12).

Fig. 11 presents the results of the geometrical features obtained for test conditions 1 and 3, round dimples. In both inspected conditions (S = 10.05 and 40.2%) the parameters extracted from the Abbot curve indicated that the obtained surfaces have good tribological

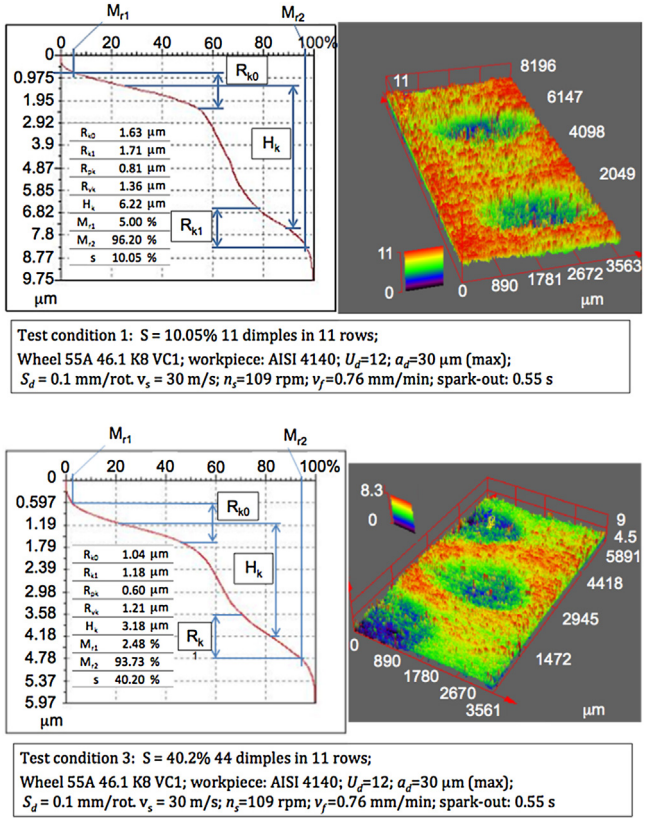

Fig. 11. R_k parameters and 3D image inspection of round dimples for two values of percentage of textured area (S).

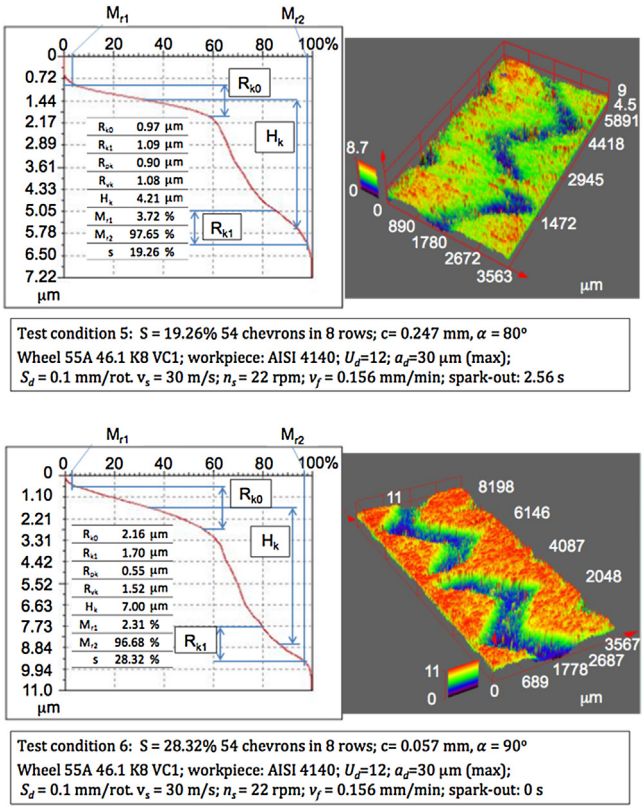

Fig. 12. R_k parameters and 3D image inspection of chevrons for two values of percentage of textured area (S).

potential, as the obtained R_{pk} (running surface roughness) values are smaller than the R_{vk} (lubricant capacity indicator) ones. In the 3D microscope inspections, a decrease in the pocket depth, from 6.79 to 3.96 µm, was observed when the percentage of texture area was increased. The same speed ratio (11) was used in both test conditions, but the higher number of dimples per row (44 *versus* 11) in condition 3 was achieved by increasing the number of features in the wheel, from 1 to 4, during patterning dressing. The wheel was dressed at the same rotation speed in both tests (1199 rpm), thus the frequency of the dressing tool displacement had to be increased four times per wheel revolution to generate the four features in the wheel surface. That fact leaded to a reduction of the achieved feature depth in the wheel surface, due to the select piezo displacement amplification. This problem could be overcome by increasing dressing depth of cut during wheel patterning, respecting piezo amplifier limits.

The same analysis was performed for the chevron pattern, test conditions 5 and 6, as depicted in Fig. 12. The same R_{pk}/R_{vk} ratio was intended. Best ratio and the deepest structure were observed in the test condition 6. The reduction of the pattern depth with the increase of the textured area was not clearly identified. The higher textured area for the chevron patterns were obtained by varying the chevron thickness *c* and the chevron angle α, with a less impact on the piezo tool displacement frequency during patterning dressing if compared to the round dimples strategy.

3. Production of micro features using a grinding wheel with positioned grains

The manufacturing of micro features was done via a completely different approach than presented in section 2. Instead of producing macro features by dressing a conventional wheel, a superabrasive grinding wheel manufactured with a defined grain pattern was used to produce micro features. The method will be described in the following subsections.

3.1. Method

To produce the micro features, a grinding wheel with defined grain pattern was employed, opposed to a conventional grinding wheel with common, random grain distribution. Grinding wheels with defined grain patterns have the advantage that the position of every grain is known. Thus, deterministic structures can be manufactured, as the material removal of every grain is a priori known. The manufactured structures applying this approach are composed by multiple single grain scratches. The setup of this method can be seen in Fig. 13.

Low relative speeds between grinding wheel and workpiece are necessary for this approach. Low relative speeds can be achieved via high workpiece speeds. As the given machine axes were not able to provide sufficiently high workpiece speeds, the workpiece movement in both directions was carried out by an x/y-linear driving unit. A rising ratio of grinding wheel speed to workpiece speed results in more grain-surface contacts per workpiece area and hence in denser patterns and intersecting scratches. When the ratio reaches a certain value, the surface will be a common ground surface. Using the linear driving unit, workpiece speeds of 1 m/s can be reached for both directions, being sufficient to produce defined structures. If the grinding machine is capable of achieving high workpiece speeds, no additional investment for a linear driving unit is necessary.

The most important aspect of the approach is the grinding wheel with defined grain pattern. Such grinding wheels were developed in the past to improve the grinding process in terms of chip formation and energy reduction (see for instance Aurich et al., 2003; Herzenstiel et al., 2009). Such wheels can be used for structuring, as the positions of the grains are known. In combination with the control of the kinematics of the process, it is possible to mathematically describe the paths of every single grain. Thus, deterministic structures can be manufactured.

The galvanic-bonded grinding wheel presented in this paper provided a nominal grain line distance of 4 mm in circumferential direction and 1.7 mm in axial direction (see Fig. 13). The number of grain lines in axial direction was 17. CBN was used as abrasive with a nominal grain size of B251. In addition to the guidelines (ISO 6106), the grains were specially filtered and sorted to achieve a uniform distribution of grain size and shape. Despite this additional sieving process, the height distribution of the grains was not uniform. However, a uniform height of the grains is mandatory, as the depth of the single scratches varies according to the differences in the grain height. The intended structure depths were 2–10 µm. As a consequence, the variation of grain height had to be extremely small.

The grain heights were measured by means of a digital fringe projection system. The height of a single grain was identified by the determination of its highest protruding point. This point was determined by placing multiple contour lines across the grain topography measurements, see Fig. 14. In addition, the roundness error of the grinding wheel had to be taken into account, as well as the characteristic distribution of the bond thickness of galvanically bonded wheels. The thickness of the bond is thinnest in the middle of the abrasive layer in axial direction and becomes thicker towards the edges of the grinding wheel. To gain this data, an eddy current sensor was used. The sensor was positioned below the grinding wheel. The wheel was moved in axial direction back and forth to acquire the bond surface profile. The wheel was then turned and the next profile was measured, without moving the eddy current sensor. This procedure was repeated eight times. Hence, eight positions of the bond surface profile in a distance of 45° to each other

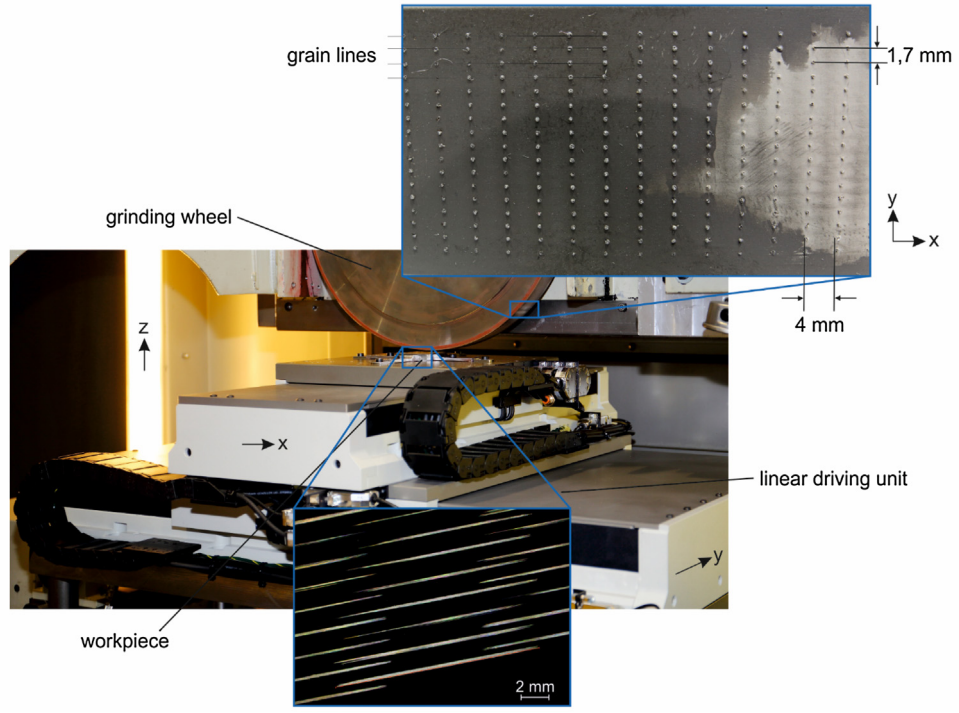

Fig. 13. Test setup for texturing.

were examined. As the position of the sensor was held constant, it was possible to relate the acquired values to each other and use them as offsets and to determine the roundness error.

The roundness error of the grinding wheel was about 12 μm, the variation of bond thickness about 26 μm from the innermost circumferential grain (L8) line to the outermost (L1 and L17), see sample measurement in Fig. 14. In total the protrusion of 136 grains was determined using the digital fringe projection system. The values of the bond thickness and roundness measurements were used as an offset to those values. The grain heights varied from 60 to 190 μm (corrected values) with an average value of 127 μm and a standard deviation of 25 μm.

The wheel was dressed using a diamond dressing wheel to achieve a uniform grain height distribution. After this dressing operation, the grain protrusion heights were measured again. To assure a uniform grain height, the grains were dressed down to a protrusion height of 50 μm. The resulted standard deviation of the grain protrusion height was equal to 3 μm.

3.2. Kinematics

The parameters that can be chosen are the grinding wheel speed, the speed of the workpiece in x and y directions and the depth of cut. In this section, the basic equations will be derived to demonstrate how the control of the kinematics works.

Initially, a workpiece speed of 0 is considered. The length of a scratch is then determined by the contact arc resulting from the radius R_d of the wheel, the grain protrusion height h and the depth of cut a_e (see Fig. 15). The contact angle α is then given by:

$$\alpha = \cos^{-1}\left(\frac{R_d + h - a_e}{R_d + h}\right) \tag{6}$$

The half-length of the scratch X_1 is the given by

$$X_1 = \sin\alpha \cdot (R_d + h) \tag{7}$$

With the angular velocity of the grinding wheel ω the contact time T_c for the scratch is given by

$$T_c = 2 \cdot \frac{\alpha}{\omega} \tag{8}$$

With the contact time T_c at hand the change of the scratch dimensions in x and y-direction (X_v and Y_v) depending on the workpiece speed in the respective directions v_x and v_y can be calculated:

$$X_v = T_c \cdot v_x \tag{9}$$

$$Y_v = T_c \cdot v_y \tag{10}$$

The final dimension of a scratch in y direction corresponds to Y_v and in x direction it corresponds to X_c, where X_c is

$$X_c = 2 \cdot X_1 + X_v \tag{11}$$

These basic equations were expanded taking grain positions, grain shapes and grain dimensions into account. The structures can be calculated based on grain positions, grain dimensions, velocity of the grinding wheel and the workpiece and depth of cut. Based on the equations, a simulation tool with a graphic user interface based on Matlab was developed. This simulation can calculate:

- The required speeds of the grinding wheel and the workpiece in the two directions and depths of cut with a given grinding wheel pattern to manufacture a desired workpiece structure,
- The resulting workpiece structure in dependence of a given wheel pattern and given speeds as well as depth of cut or
- The required grinding wheel pattern in dependence of desired workpiece structures.

3.3. Results

3.3.1. Possibilities and limitations

As mentioned before, the structures on the workpieces are a composition of single grain scratches. The shape of the single scratches is tied to the shape of the grains of the grinding wheel.

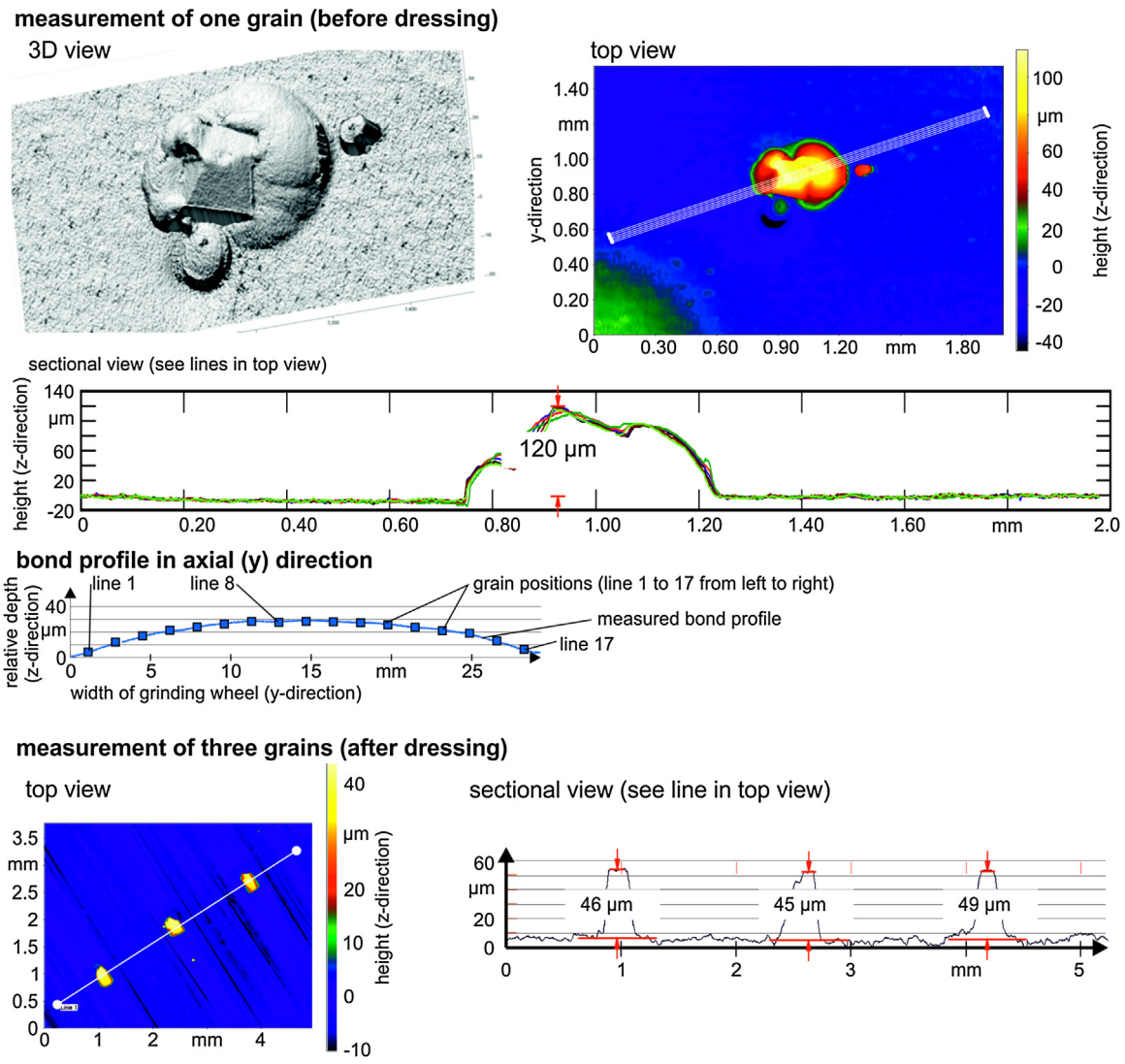

Fig. 14. Grain topography measurements.

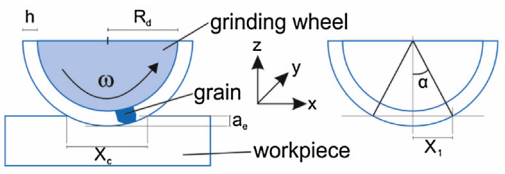

Fig. 15. Process kinematics.

This is due to the fact that the geometry of single grain scratches is a reflection of the grain shapes (Aurich and Steffes, 2011). With a given pattern of the grinding wheel at hand the structures themselves are defined by the kinematics of the process. Thus, the chosen pattern of the grinding wheel limits the possible structures to be manufactured. However, the possible variations of the structures with one specific pattern are still manifold. Some structures that can be manufactured using the presented prototype grinding wheel are shown in Fig. 16. In general, the depth of cut defines the depth of the structures. Moreover, a higher depth of cut results into a longer contact time and hence in longer scratches. The influence of the three speed parameters is more complex. The composition of the speed of the workpiece in x and y direction (v_x and v_y) is a speed vector and could also be realized by only one movement of the workpiece. Instead of the two-axle linear driving unit used in this study, a turntable, providing the required straightness and stiffness, could be implemented below a one-axle driving unit.

Generally speaking, a higher speed in x-direction results in a longer scratch in this direction in up-grinding mode. For down grinding X_v in Eq. (9) turns negative, as the total contact time becomes shorter, resulting in shorter scratches. For the y-component, a higher speed results into longer scratches for both up- or down-grinding. A higher grinding wheel speed results in shorter scratches in x-direction and shorter scratches in y-direction in the up-grinding mode. In the down-grinding mode the influence in y-direction stays the same, for the x-direction higher grinding wheel speeds result into longer scratches.

However, not only the length of the scratches in x- and y-direction can and is influenced by the kinematics but also the arrangement of them or the distance to each other, i.e. the structures. These correlations of the kinematics enable a large variety of possible structures with only one grinding wheel pattern at hand. Generally speaking, with up-grinding the structures are more dense and overlapping than for the down-grinding mode.

3.3.2. *Evaluation of the structures*

The structures were evaluated by means of 2D and 3D measurement techniques. The macroscopic properties of the structures, i.e.

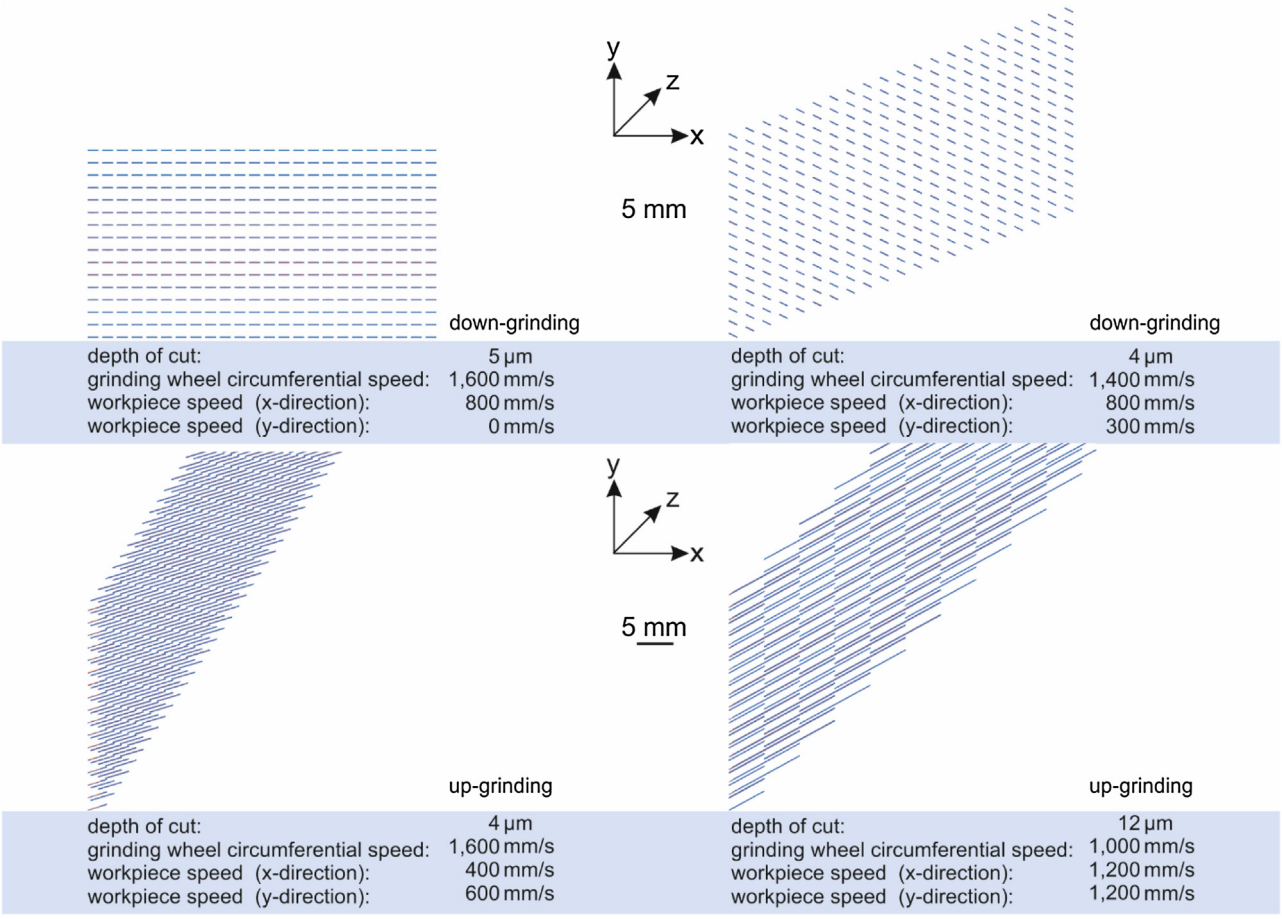

Fig. 16. Some possible structures that can be manufactured using the presented prototype grinding wheel.

the length, width and uniformity of the structures, were evaluated using a standard light microscope. Example measurements of the length and width can be seen in Fig. 17.

The microscopic properties, i.e. the depth of structures and burr measurement, were acquired via the digital fringe projection system that was also used to measure the grain protrusion heights. With the system used (MicroCAD plus from GFM) it was possible to measure the manufactured samples directly without the producing non-reflective replicas that can distort the measurement. The vertical resolution of the system was 50 nm and the lateral resolution 700 nm. The depth of the structure was measured by defining a rectangular field inside a scratch. The software determines the average depth value inside this rectangle relative to the surface of the sample. In contrast to the method of placing intersecting lines through the scratches and determining the depth of the scratches for each line, this method holds the advantage to be less subjective, to include maximum and minimum values at once and hence to obtain a representative average value with one measurement only. As the burrs exhibit small areas, this method could not be used to evaluate those. Intersecting lines were used to obtain the values of the maximum burr height per scratch, similar to the determination of grain protrusions (see Fig. 17).

3.3.3. Structure properties

An exemplary structure is evaluated in this paper to illustrate the capability of the new approach. The employed material for the workpiece was soft construction steel (200 HV 0.3). The specimens were polished before manufacturing the structures to assure a high flatness. The grinding wheel speed was 1400 mm/s and the speed in x direction 800 mm/s. Down grinding mode was applied. No motion in y direction was used. The set depth of cut was 4 µm. The resulting structure is shown in Fig. 17, right. The blank spots that are visible result from either broken out grains on the grinding wheel or from grains with protrusion heights that were below the set depth of cut.

In Fig. 18 the distribution of the depth of the scratches and the respective length of the scratches is shown. A total of 61 scratches were examined for this structure; 83 for burr measurement. It also includes the curve that represents the ideal depth a scratch of the respective length would have, based on the given kinematics. No uniform distribution of the length and depth of the scratches was achieved. The average value of the length was 1,055 µm at a standard deviation of 198 µm. The average value of the depth was 2.6 µm at a standard deviation of 1.1 µm. The structure density, i.e. the area of scratches compared to the surface area, was about 2.7 % according to the average value of the length of 1,055 µm.

Different lengths of scratches result from different grain protrusion heights (see Section 3.1: Method). The differing depths are also a result of the differing grain protrusion heights. In addition, they are a result of the material removal behavior. All grains undergo three phases: the elastic, the plastic and the chip removal phase (Klocke, 2009). In the first phase, the material is elastically deflected, no material is removed. In all three phases those elastic deflections exist. In the second phase, the material is plastically deformed but no chip is formed. Those plastic deformations also exist in the third phase and are responsible for the formation of burrs. In the last phase, a chip is formed after the so-called grain cutting depth T_μ is achieved. The grain cutting depth depends on the material properties, i.e. the yield point, as well as the cutting

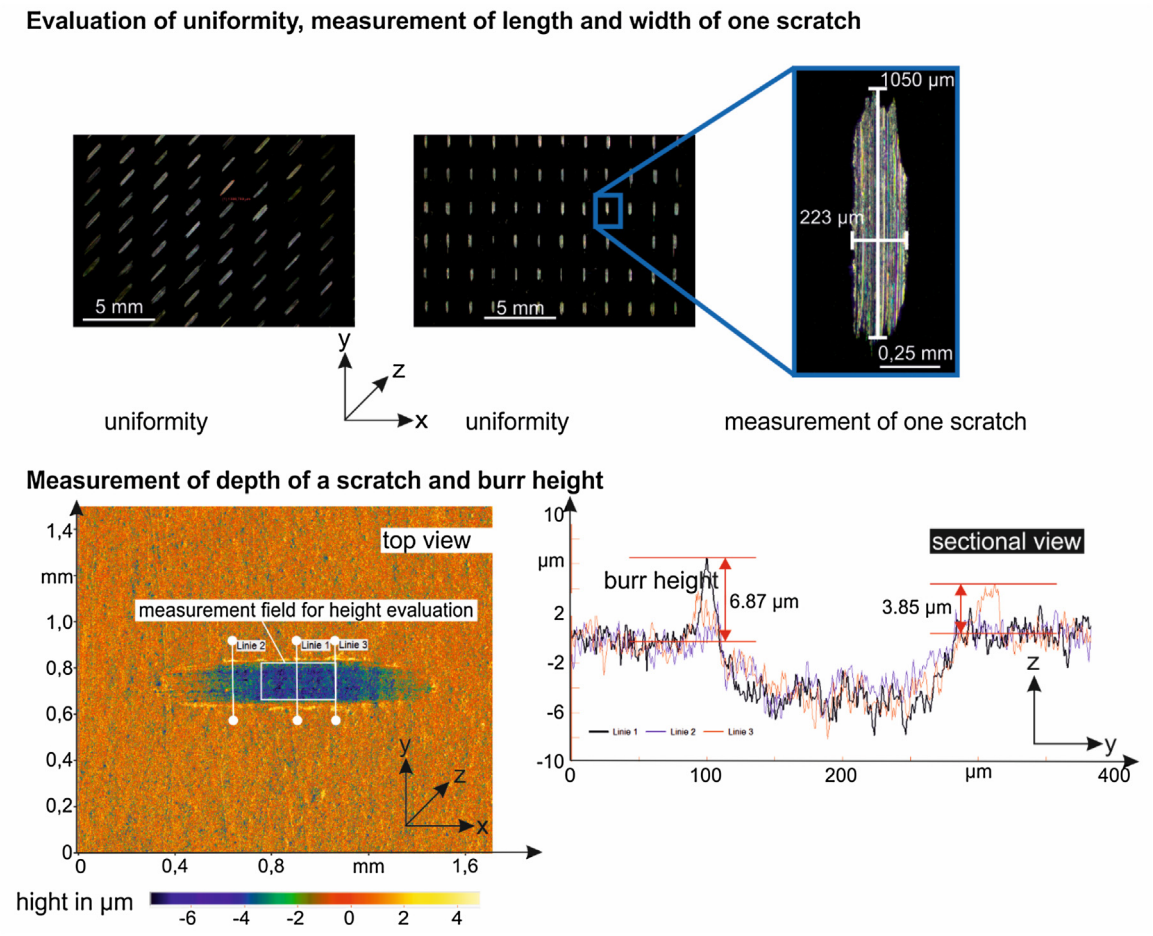

Fig. 17. Evaluation of the produced scratches.

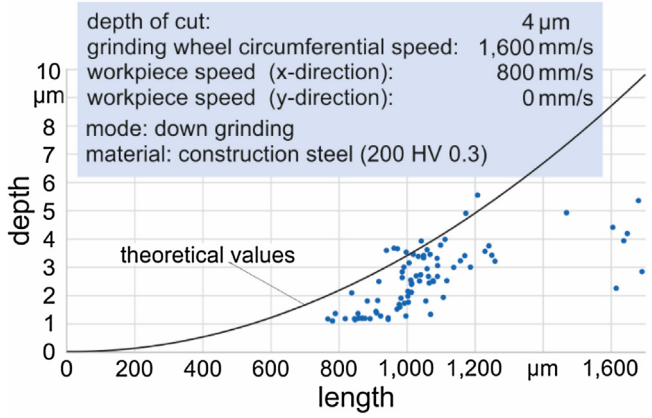

Fig. 18. Results of distribution of the depth of the scratches and the respective length.

speed and the grain shapes. A lower yield point favours smaller grain cutting depths, i.e. shorter phases I and II, as well as higher cutting speeds. Recent work of Rasim et al. (2015) showed that blocky, blunt grains, as they prevail for this method, favour lower grain cutting depths. Higher grain cutting depths result in a smaller ratio of the achieved depths of the scratches to the set cutting depth.

To evaluate this ratio, it was assumed that a contact grain-workpiece results in a visible change of the surface even in the first, elastic material removal phase. This assumption can be made as the workpieces are polished to mirror quality before the manufacturing of the structures and hence are highly sensitive. In addition, as shown in recent works, phase I is very short compared to the complete scratch length (Rasim et al., 2015). Based on the measured length of a scratch, the set depth of cut per scratch can be calculated using the derived equations (see Section 3.1: Method – Kinematics). For the average length of the scratches (1,055 µm), a set depth of cut of 3.8 µm results. With the average depth of the scratches of 2.6 µm, the resulting ratio is 0.68. The difference accounts for the elastic material behavior, plastic deformations, i.e. material gliding under the grain, as well as elastic deflections of the whole setup. The latter appears due to limited stiffness of the wheel clamping, the clamping of the workpiece, the linear driving unit and its connection to the machine bed, etc.

Preliminary measurement of the forces during the manufacturing of the structures revealed forces in normal direction of up to 500 N. It can hence be assumed that there is an influence of the stiffness of the setup. Force measurements during the manufacturing will be evaluated in depth in future works.

As shown in Fig. 18, some scratches exhibit depths slightly exceeding the theoretical values based on purely geometric-kinematic consideration according to their length. This could be ascribed to measurement errors or to the material removal itself. It could be possible that material agglomerates on the tip of the grain and removes material itself and hence increases the grain penetration depth. In other words, a built-up edge was formed. This phenomenon will be investigated further by broadening the researched material. When grinding very hard and brittle material, no built-up edge can be formed and hence the values of the measured depths must be below the theoretical values.

The plastic deformation of the material is also reflected in the formation of burrs. The average burr height of the sample structure was 4.9 μm, while the maximum burr height measured was 12 μm and the minimum 0.4 μm; 31 of the examined 83 scratches did not exhibit any detectable burrs. Burrs result into increased friction. Thus, they have to be removed for the targeted application of the structures, i.e. sliding components. However, the burr formation is closely tied to the material properties. Preliminary results when manufacturing structures in the hardened heat-treated steel AISI 4140 (635 HV 0.3) resulted in significantly reduced burr formation compared to the soft construction steel examined in this study. This will be further investigated in future works.

4. Conclusion

In this paper, two approaches to manufacture structured surfaces via grinding were presented. The first approach is for the production of macro features using random grain distribution wheel, specially conditioned during dressing and the second is for the production of micro features using grinding wheels with defined grain pattern.

The main conclusions for the first approach are:

- Theoretically designed patterns such as dimples and chevrons can be transferred to the workpiece, varying the number and the percentage of textured area.
- The method allowed the production of structured surfaces with macro features in conventional CNC machines using conventional abrasive wheels.
- The machine setup for the new process is quite simple and does not require any automation, CNC or major software modification.
- The obtained structured surfaces can be tailored to result in different roughness values in the textured and non-textures regions of the part.
- Larger and deeper patterns favour the maintenance of the engagement factor (self-synchronization effect) between the grinding wheel and workpiece during texturing, resulting in less deformation of the geometry and avoiding pattern overlap.

The main conclusions for the second approach using grinding wheels with defined grain pattern:

- With the presented approach, it is possible to produce micro features in a wide variety. The structures are a composition of single grain scratches; hence the shape of the single scratches is a result of the single grain geometries.
- The simulation tool developed allowed adequate control of the textures.
- Deviations between the simulated and manufactured structures are mainly lower depths of the single scratches. This can be led back to material removal mechanisms as well as deflections in the setup.
- Side burrs were measured that possibly could impair the tribological performance of the structures. Burr formation is expected to be minimized when grinding hardened steels. Potential remaining burrs have to be removed with appropriate methods. This will be examined in future works.

General guidelines for method selecting are based on the type and dimensions of the desired textured feature:

- The patterning using a random grain distribution wheel will be used to produce macro features, with high geometry selection flexibility. In that case, virtually all types of patterns can be produced, typically with minimum feature width equal to the dressing tool width, by imprinting a negative of the desired pattern on the wheel surface during dressing. High complex features can be decoupled by the pattering software and transferred as a controlled path trajectory for the dressing tool to form the desired feature. Patterns can be easily removed by redressing the wheel with a fixed depth of cut, in preparation for a new pattern imprint.
- The pattern with grinding wheel with positioned grains will be used to produce micro features of a size of an abrasive grain, with low geometry selection flexibility. By adjusting the kinematics, variations in size and orientation of the scratches can be performed. Major pattern arrangements modifications implies on the manufacturing of a new grinding wheel.

The capability of both approaches to manufacture structured surfaces was demonstrated in this paper. The main advantage of the approaches compared to common structuring methods such as laser ablation or high-precision machining is the short process time. The process time to produce one structured workpiece with macro features is the same as the one for regular grinding. Wheel patterning occurs during the regular dressing stroke and workpiece patterning occurs simultaneously with the stock removal in the grinding cycle. The shortest grinding cycle tested in this paper was 2 s; the process time for adding micro features on a functional area on flat surfaces of about 1500 mm^2 as presented here is only 0.063 s.

In future works, the tribological performance of the workpieces will be analyzed. This will be done via a hydrodynamic test-bed (macro features) and a pin-on-disc tribometer (micro features).

Acknowledgements

The research presented in this paper was funded by the Deutsche Forschungsgemeinschaft-DFG (AU 185/34-1) and the CAPES (Grant # 23038.006062/2012-45 Bragecrim 1918/2012) as part of the Brazilian-German Collaborative Research Initiative on Manufacturing Technology (BRAGECRIM).

References

Aurich, J.C., Steffes, M., 2011. Single grain scratch tests to determine elastic and plastic material behavior in grinding. Adv. Mater. Res. 325, 48–53.
Aurich, J.C., Braun, O., Warnecke, G., 2003. Development of a superabrasive grinding wheel with defined grain structure using kinematic simulation. CIRP Ann. Manuf. Technol. 52 (1), 275–280.
Bruzzone, A.A.G., Costa, H.L., Lonardo, P.M., Lucca, D.A., 2008. Advances in engineered surfaces for functional performance. CIRP Ann. Manuf. Technol. 57 (2), 750–769.
Cho, C., Kim, H., Jeong, S., Baek, S., Seo, J., Han, D., Kim, K., Park, Y., Yoo, S., Lee, J., 2013. Random and V-groove texturing for efficient light trapping in organic photovoltaic cells. Sol. Energy Mater. Sol. Cells 115, 36–41.
Costa, H.L., Hutchings, I.M., 2007. Hydrodynamic lubrication of textured steel surfaces under reciprocating slinding conditions. Tribol. Int. 40 (8), 1227–1238.
Costa, H.L., Hutchings, I.M., 2009a. Effects of die surface patterning on lubrication in strip drawing. J. Mater. Process. Technol. 209 (3), 1175–1180.
Costa, H.L., Hutchings, I.M., 2009b. Development of a maskless electrochemical texturing method. J. Mater. Process. Technol. 209 (8), 3869–3878.
DIN ISO 6106: Schleifmittel – Überprüfung der Korngrößen von Diamant oder kubischem Bornitrid. DIN Deutsches Institut für Normung e.V., (2006).
DIN 4776: Determination Of Surface Roughness Parameters Rk, Rpk, Rvk, Mr1, Mr2 Serving To Describe The Material Component Of Roughness Profile.
Denkena, B., Köhler, J., Wang, B., 2010. Manufacturing of functional riblet structures by profile grinding. CIRP J. Manuf. Sci. Technol. 3 (1), 14–26.
Galda, L., Pawlus, P., Sep, J., 2009. Dimples shape and distribution effect on characteristics of Stribeck curve. Tribol. Int. 42 (10), 1505–1512.
Herzenstiel, P., Kirsch, B., Aurich, J.C., 2009. Spezialwerkzeug zum Trocken- und Nassschleifen. Diamond Bus. 8 (4), 16–23.
Hilgenberg, K., Steinhoff, K., 2015. Texturing of skin-pass rolls by pulsed laser dispersing. J. Mater. Process. Technol. 225, 84–92.
ISO 13565-2: Geometrical Product Specifications (GPS) – Surface texture: Profile method; Surfaces having stratified functional properties – Part 2: Height characterization using the linear material ratio curve. 6p.
Ibatan, T., Uddin, M., Chowdhury, M.A.K., 2015. Recent development on surface texturing in enhancing tribological performance of bearing sliders. Surf. Coat. Technol. 272, 102–120.

Klocke, F., 2009. Principles of cutting edge engamement. In: Manufacturing Processes 2. Grinding, Honing, Lapping. Springer-Verlag, Berlin, pp. 3–16.
Mourier, L., Mazuyer, D., Lubrecht, A.A., Donnet, C., 2006. Transient increase of film thickness in micro-textured EHL contacts. tribology international 39/12 – interactions of tribology and the operating environment. In: Proceedings of the 32nd Leeds-Lyon Symposium on Tribology, Lyon, France, pp. 1745–1756.
Oliveira, J.F.G., Dornfeld, D.A., 2001. Application of AE contact sensing in reliable grinding monitoring. CIRP Ann. Manuf. Technol. 50 (1), 217–220.
Oliveira, J.F.G., Bottene, A.C., França, T.V., 2010. A novel dressing technique for texturing of ground surfaces. CIRP Ann. Manuf. Technol. 59 (1), 361–364.
Rasim, M., Mattfeld, P., Klocke, F., 2015. Analysis of the grain shape influence on the chip formation in grinding. J. Mater. Process. Technol. 226, 60–68.
Silva, E.J., Oliveira, J.F.G., Salles, B.B., Cardoso, R., Reis, V.R.A., 2013. Strategies for production of parts textured by grinding using patterned wheels. CIRP Ann. Manuf. Technol. 62 (1), 355–358.
Silva, E.J., Bottene, A.C., Oliveira, J.F.G., Atoatte, A., Rodrigues, A.S., 2016. Grinding process for profiled texturing. CIRP Ann. Manuf. Technol. 65 (1), 337–340.
Stępień, P., 1989. Generation of regular patterns on ground surfaces. CIRP Ann. Manuf. Technol. 38 (1), 561–566.
Stępień, P., 2011. Deterministic and stochastic components of regular surface texture generated by a special grinding process. Wear 271, 514–518.
Uhlmann, E., Bäcker, C., Schröer, N., 2013. Surface structuring using kinematic modulation in grinding. Prod. Eng. Res. Dev. 7 (4), 373–381.
Wang, X., Kato, K., Adachi, K., Aizawa, K., 2003. Loads carrying capacity map for the surface texture design of SiC thrust bearing sliding in water. Tribol. Int. 36 (3), 189–197.
Wang, F., Zhang, X., Wang, L., Jiang, Y., Wei, C., Zhao, Y., 2015. Pyramidal texturing of silicon surface via inorganic-organic hybrid alkaline liquor for heterojunction solar cells. J. Power Sources 293, 698–705.
Zhang, H., Qin -g, L., Hua, M., Dong -n, G., Chin, K.-S., 2015. A tribological study of the petaloid surface texturing for Co–Cr–Mo alloy artificial joints. Appl. Surf. Sci. 332, 557–564.
Zhang, J., Meng, Y., 2012. A study of surface texturing of carbon steel by photochemical machining. J. Mater. Process. Technol. 212 (10), 2133–2140.